JOURNAL OF SYNCHROTRON RADIATION

ISSN 1600-5775

Received 6 July 2017
Accepted 20 October 2017

Edited by M. Zangrando, IOM-CNR and Elettra-Sincrotrone, Italy

Keywords: X-ray free-electron laser; soft X-rays; arrival timing diagnostics.

Single-shot arrival timing diagnostics for a soft X-ray free-electron laser beamline at SACLA

Shigeki Owada,[a]* Kyo Nakajima,[b,a] Tadashi Togashi,[b,a] Tetsuo Kayatama[b,a] and Makina Yabashi[b,a]

[a]RIKEN SPring-8 Center, Sayo-cho, Sayo-gun 679-5148, Japan, and [b]Japan Synchrotoron Radiation Research Institute, Sayo-cho, Sayo-gun 679-5198, Japan. *Correspondence e-mail: osigeki@spring8.or.jp

Arrival timing diagnostics performed at a soft X-ray free-electron laser (FEL) beamline of SACLA are described. Intense soft X-ray FEL pulses with one-dimensional focusing efficiently induce transient changes of optical reflectivity on the surface of GaAs. The arrival timing between soft X-ray FEL and optical laser pulses was successfully measured as a spatial position of the reflectivity change. The temporal resolution evaluated from the imaging system reaches ~10 fs. This method requires only a small portion of the incident pulse energy, which enables the simultaneous operation of the arrival timing diagnostics and experiments by introducing a wavefront-splitting scheme.

1. Introduction

To conduct ultrafast pump–probe experiments, arrival timing diagnostics between free-electron laser (FEL) and optical laser pulses are required to compensate for possible arrival timing jitter between these pulses. For this purpose, new techniques which probe the transient changes of the optical reflectivity or transmissivity of semiconductors induced by intense soft and hard X-ray FEL irradiation have been developed (Maltezopoulos *et al.*, 2008; Gahl *et al.*, 2008; Krupin *et al.*, 2012; Harmand *et al.*, 2013; Bionta *et al.*, 2014). For the hard X-ray region, one-dimensional X-ray focusing was applied to the reduction of an XFEL pulse energy required for producing transient changes below 10 μJ at a photon energy of ~10 keV (Sato *et al.*, 2015). Furthermore, a beam branching method using a transmission grating enabled pump–probe experiments to be performed simultaneously with the arrival timing diagnostics (Katayama *et al.*, 2016).

However, the method, based on an amplitude-splitting scheme, cannot be directly applied in the extreme-ultraviolet (EUV) and soft X-ray regions due to the lack of transmission beam splitters that have high diffraction efficiency with reasonable transmissivity. We note that transmissive timing monitoring is available at ~1000 eV (Beye *et al.*, 2012), while it becomes difficult below a few hundred eV due to a decrease of the transmissivity

On the contrary, a wavefront-splitting scheme is applicable to beam branching even in the EUV and soft X-ray regions. In this paper we investigate the feasibility of arrival timing diagnostics that use only a small portion of the incident XFEL beam. In §2 we describe an experimental setup and results with one-dimensional focusing of soft X-ray FEL pulses. Following the result with a partial beam condition in §3, we discuss possible plans to extend this method to simultaneous

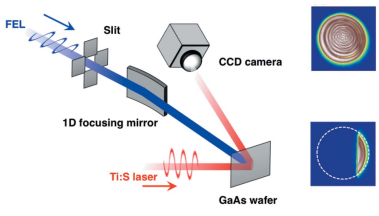

operation of experiments and arrival timing diagnostics by introducing the wavefront-splitting scheme in §4.

2. Experiment with one-dimensional focusing

As a first step, we performed a basic test with one-dimensionally focused soft X-ray FEL pulses. We used a soft X-ray FEL beamline BL1, which employs a dedicated 800 MeV linac, the SCSS+ (Owada *et al.*, 2018), at the SACLA facility (Ishikawa *et al.*, 2012). Fig. 1(*a*) depicts the detailed setup, which is similar to the setup described by Maltezopoulos *et al.* (2008). To obtain a high excitation efficiency, the incident X-ray beam at a photon energy of 100 eV with a ∼8 mm top-hat profile (Fig. 1*b*) was one-dimensionally focused onto a mirror-polished GaAs wafer (30 mm × 30 mm) to a spot size of 200 µm full width at half-maximum (FWHM). A typical FEL pulse energy was reduced from the original output of 80 µJ to ∼20 µJ by using attenuators combined with Zr foils and N_2 gas. The FEL fluence on the surface of the GaAs wafer was estimated as ∼4 mJ cm^{-2}, which is a sufficiently high intensity to induce a transient reflectivity change. We note that we did not observe any permanent damage on the surface after 12 h irradiation.

Synchronized Ti:sapphire laser pulses with a photon energy of 1.55 eV and a pulse duration of 50 fs were focused using a pair of cylindrical lenses to a spot size of 100 µm × 2000 µm. The optical beam irradiated the GaAs wafer with an incident angle of 45°, and the reflected beam was detected with a visible CCD camera (OPAL-2000) that combines an imaging lens. The spatial resolution of the camera is 3.5 µm pixel^{-1}, which corresponds to a temporal resolution of 8.3 fs pixel^{-1} estimated from the optical geometry of the spatial encoding method.

Fig. 2 shows single-shot CCD images in different optical delays that were controlled with a delay stage for the optical laser pulse. The optical laser pulses were vertically polarized,

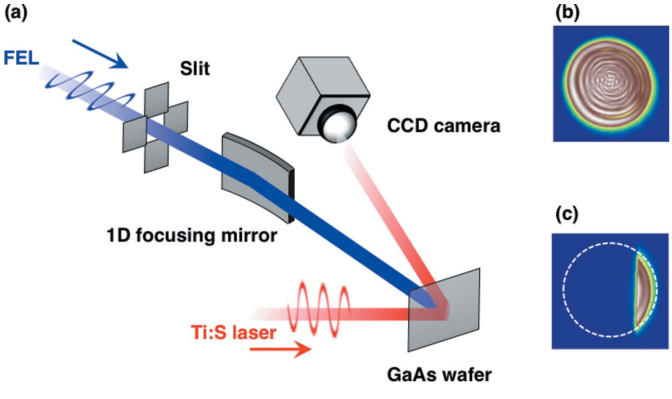

Figure 1
(*a*) Schematic of the experimental setup. The horizontally polarized soft X-ray pulses were one-dimensionally focused onto the GaAs wafer. The optical laser pulses were vertically polarized, which corresponded to the reflection of p-polarized pulses. The reflected beam was imaged onto the visible CCD camera. (*b*) Spatial profile of the incident soft X-ray FEL beam. (*c*) Spatial profile after the 1 mm-width slit. The white dashed circle depicts the incident beam size.

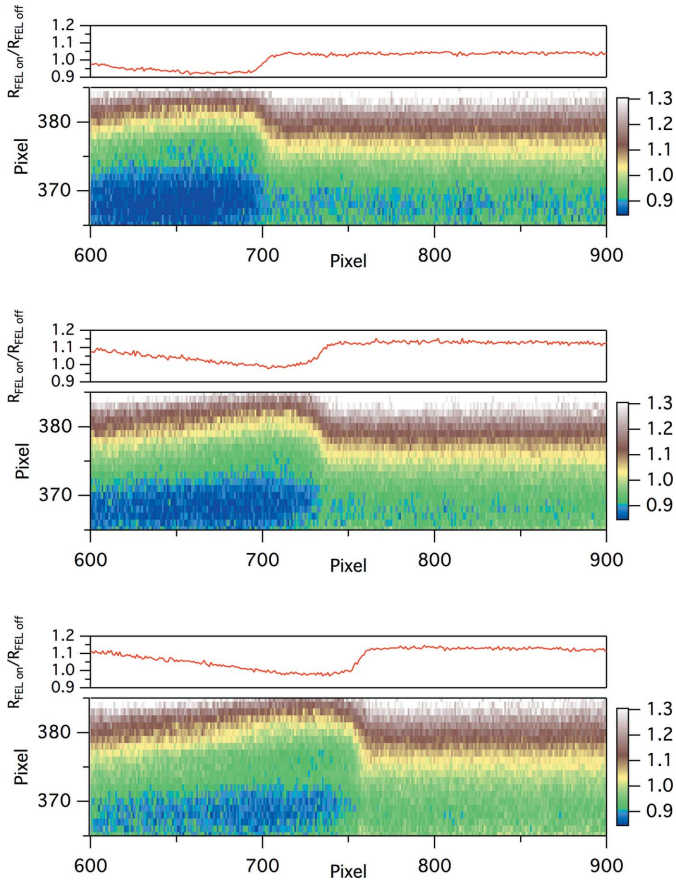

Figure 2
Normalized single-shot CCD images in different optical delays. The relative arrival timing was projected onto the horizontal axis of these images (lower image in each panel). The pixel intensity was integrated along the vertical axis between 370 and 380 pixel (upper graph in each panel).

corresponding to the reflection of p-polarization geometry. The relative arrival timing was projected onto the horizontal axis of these images. Intensities of each pixel were normalized by the background signal without soft X-ray irradiation. A smaller number of horizontal pixels indicates an arrival of the soft X-ray pulses earlier than the optical pulses. We clearly observed a reduction of reflectivity of ∼10% to ∼15% after the soft X-ray pulses are irradiated. An edge position of the reflectivity change was evaluated using the software package running on the SACLA HPC system [*Timing Monitor Analyzer* (*TMA*); Nakajima *et al.*, 2018]. Under the present conditions, more than 97% of images are successfully analyzed using *TMA*. Fig. 3 shows the dependence of a 1000-shot-averaged edge position with respect to the delay time between the soft X-ray and the optical pulses. The pixel to the arrival timing conversion coefficient was determined to be 8.6 (2) fs pixel^{-1}, which is consistent with that derived from the optical geometry.

Next, we investigated the dependence of the reflectivity change on polarization. Fig. 4(*a*) shows a typical single-shot CCD image when the horizontally polarized optical pulses, which correspond to s-polarization, were irradiated. The reduction of reflectivity was not clearly observed when

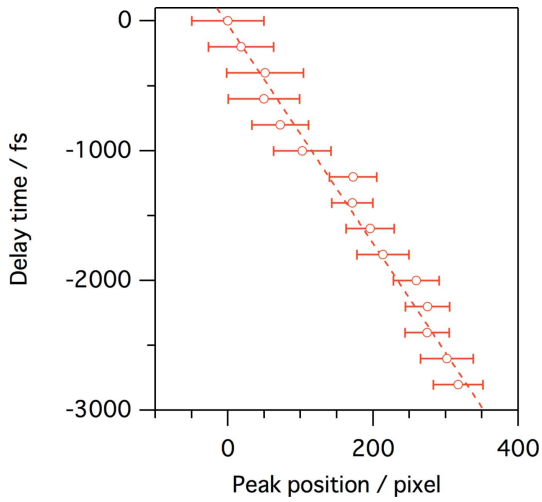

Figure 3
Dependence of the 1000-shot-averaged edge position on the CCD images with respect to the delay time between the soft X-ray and the optical pulses. The horizontal bars represent the 2σ width of the edge positions to be evaluated.

compared with the p-polarization condition in Fig. 2. The reflectivity difference can be explained using the Drude model. First, the free-carrier density (N) created at the surface of a GaAs wafer is estimated (Harmand *et al.*, 2013; Katayama *et al.*, 2016),

$$N = \frac{E_0}{2AdE_\mathrm{b}}\left\{1 - \exp\left[\frac{-d}{\cos(\theta_i)\mu}\right]\right\}, \qquad (1)$$

where E_0, E_b, A, θ_i, d and μ are the incident pulse energy, the band gap energy of GaAs, the spot size, the incident angle between the soft X-ray FEL beam and the sample normal, the sample thickness, and the penetration depth at 100 eV, respectively. Here, we assumed that the sample thickness equals the penetration depth at 1.55 eV, and free-carriers were distributed uniformly in the GaAs. Under our experimental conditions, the free-carrier density was calculated to be $\sim 10^{20}$ cm^{-3}.

The refractive index at a wavelength of λ is described using the plasma frequencies, ω_e and ω_h,

Table 1
Typical parameters of GaAs at 300 K.

	Electron	Hole
Effective mass	$0.067m_\mathrm{e}$	$0.40m_\mathrm{e}$
Mobility (cm^2 V^{-1} s^{-1})	8500	400
Relaxation time (ps)	4.8	0.2

$$n(\lambda)^2 = n_0(\lambda)^2 - \left(\frac{\omega_\mathrm{e}}{\omega}\right)^2 \frac{1}{1 + i/(\omega\tau_\mathrm{e})} - \left(\frac{\omega_\mathrm{h}}{\omega}\right)^2 \frac{1}{1 + i/(\omega\tau_\mathrm{h})}, \qquad (2)$$

$$\omega_\mathrm{e} = \left(Ne^2/\varepsilon_0 m_\mathrm{e}\right)^{1/2}, \qquad \omega_\mathrm{h} = \left(Ne^2/\varepsilon_0 m_\mathrm{h}\right)^{1/2}, \qquad (3)$$

where ω, m_e, m_h, ε_0, τ_e and τ_h are the optical laser frequency, the electron and hole effective mass, the vacuum permittivity and the electron and hole relaxation times, respectively. The relaxation times were derived from the effective mass and the mobility. The values of these parameters are listed in Table 1 (Kasap, 2002). Using the above equations, the reflectivity of p- and s-polarized pulses are derived from the Fresnel formula. Fig. 4(*b*) shows the reflectivity of p- and s-polarized pulses at $h\nu = 1.55$ eV with respect to the free-carrier density. The ratio of the reflectivity reduction of p-polarized optical pulses is more than two times larger than that of s-polarized pulses under our experimental conditions.

3. Experiment with partial beam

As a next step, we tested an application of this method to a partial beam condition. For this purpose, a slit was used for extracting an edge of the soft X-ray beam with a width of 1 mm, which was transported to the arrival timing diagnostics system (Fig. 1*c*). The pulse energy at the sample was ~4 µJ. The beam size along the focusing direction was 70 µm (FWHM), while that along the unfocused one was 3300 µm, which corresponds to a fluence of ~2 mJ cm^{-2}. The single-shot images processed with the above algorithm are shown in Fig. 5. We observed a reflectivity change of ~8% with a successful evaluation ratio of ~98% for detection of the boundary of the reflectivity change. The single-shot relative arrival timing fluctuation for 20 min was measured to be 243 fs (RMS), as shown in Fig. 6. Again, we did not observe any

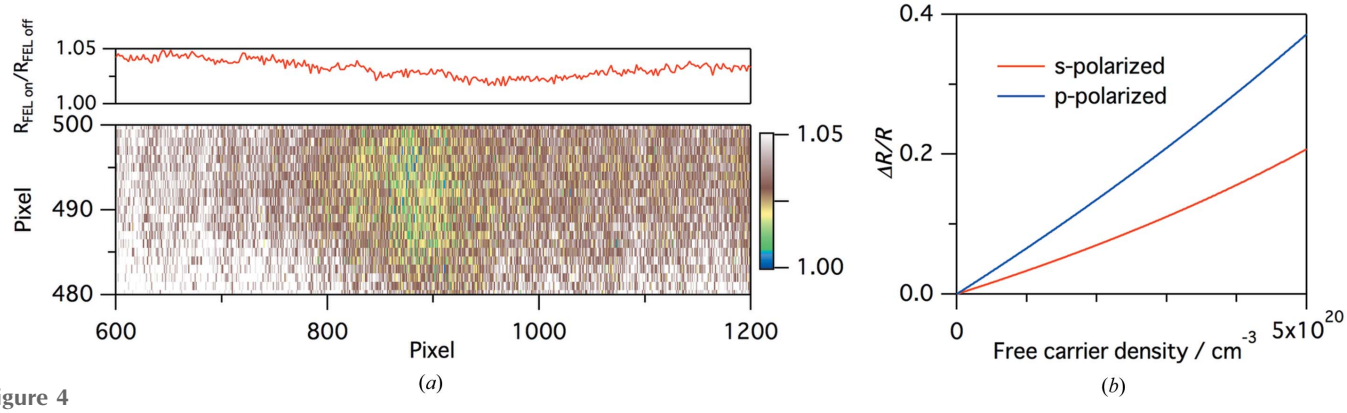

Figure 4
(*a*) Normalized single-shot CDD image for the s-polarized pulse. (*b*) Calculated ratio of reflectivity change dependent on free-carrier density. The free-carrier density under our experimental conditions is estimated to be $\sim 10^{20}$ cm^{-3}.

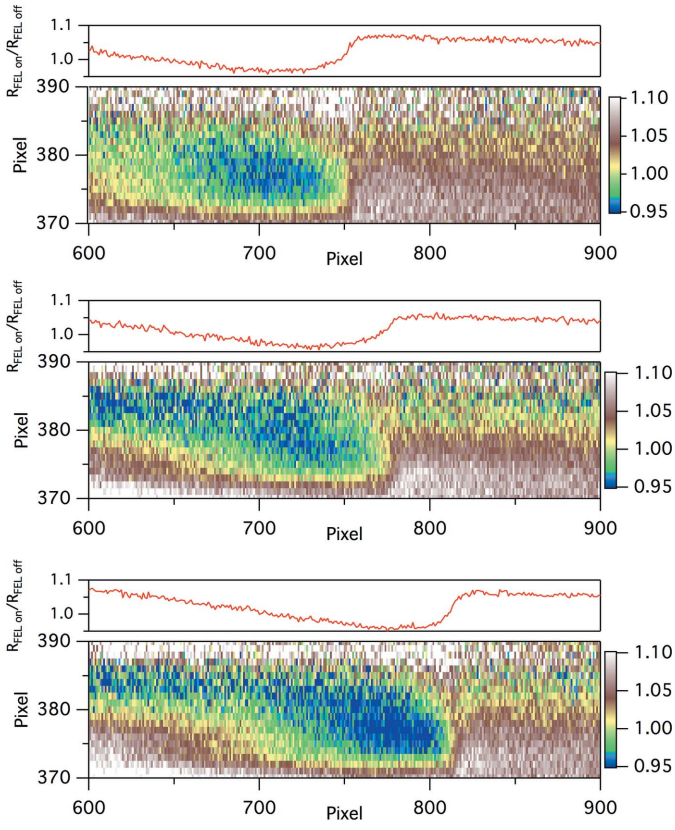

Figure 5
The normalized single-shot CCD images (lower image in each panel) and the intensity profile integrated along the vertical axis between 375 and 385 pixel (upper graph in each panel). The slit was closed to extract the edge of the soft X-ray FEL beam of 1 mm width.

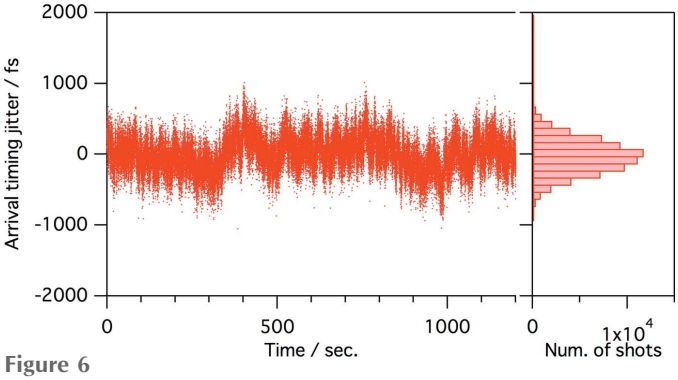

Figure 6
Variation of the arrival timing between the soft X-ray FEL and the optical laser pulses for 20 minutes (left) and histogram (right).

permanent damage on the GaAs wafer, nor substantial pointing drifts of both optical and soft X-ray pulses over 12 h.

4. Discussion

The reflectivity change is due to the plasma formation, which starts from the ionization of core electrons following the Auger process and the electron impact ionization. The practical temporal resolution is strongly affected by the pulse durations of FEL and optical lasers. In this study, we achieved ~50 fs accuracy in edge evaluation, which is comparable with the temporal resolution expected from the pulse duration of FEL/optical pulses.

We demonstrated a feasibility of the arrival timing diagnostics by using a small portion (*i.e.* a width of 1 mm from 8 mm) of the incident soft X-ray beam around the edge. Although the main beam was blocked by the slit in this setup, we can modify the optical geometry to the beam branching scheme by using a small beam-steering mirror; the mirror deflects an edge part of the incident beam to the diagnostic system, while a large portion of the beam is transported to the experimental apparatus without interference. Alternatively, the steering mirror may be substituted by a small focusing mirror that works as the first optics of the diagnostic system.

Acknowledgements

The authors are grateful to all the scientific and engineering staff of SACLA. The soft X-ray FEL experiments were performed at the BL1 of SACLA with the approval of the Japan Synchrotron Radiation Research Institute (JASRI) (Proposal No. 2017A8087).

References

Beye, M., Krupin, O. Hays, G. Reid, A. H., Rupp, D., de Jong, S., Lee, S., Lee, W.-S., Chuang, Y.-D., Coffee, R., Cryan, J. P., Glownia, J. M., Föhlisch, A., Holmes, M. R., Fry, A. R., White, W. E., Bostedt, C., Scherz, A. O., Durr, H. A. & Schlotter, W. F. (2012). *Appl. Phys. Lett.* **100**, 121108.

Bionta, M. R., Hartmann, N., Weaver, M., French, D., Nicholson, D. J., Cryan, J. P., Glownia, J. M., Baker, K., Bostedt, C., Chollet, M., Ding, Y., Fritz, D. M., Fry, A. R., Kane, D. J., Krzywinski, J., Lemke, H. T., Messerschmidt, M., Schorb, S., Zhu, D., White, W. E. & Coffee, R. N. (2014). *Rev. Sci. Instrum.* **85**, 083116.

Gahl, C., Azima, A., Beye, M., Deppe, M., Döbrich, K., Hasslinger, U., Hennies, F., Melnikov, A., Nagasono, M., Pietzsch, A., Wolf, M., Wurth, W. & Föhlisch, A. (2008). *Nat. Photon.* **2**, 165–169.

Harmand, M., Coffee, R., Bionta, M. R., Chollet, M., French, D., Zhu, D., Fritz, D. M., Lemke, H. T., Medvedev, N., Ziaja, B., Toleikis, S. & Cammarata, M. (2013). *Nat. Photon.* **7**, 215–218.

Ishikawa, T. *et al.* (2012). *Nat. Photon.* **6**, 540–544.

Kasap, S. O. (2002). *Principles of Electronic Materials and Devices*, 2nd ed. New York: McGraw-Hill.

Katayama, T., Owada, S., Togashi, T., Ogawa, K., Karvinen, P., Vartiainen, I., Eronen, A., David, C., Sato, T., Nakajima, K., Joti, Y., Yumoto, H., Ohashi, H. & Yabashi, M. (2016). *Struct. Dynam.* **3**, 034301.

Krupin, O., Trigo, M., Schlotter, W. F., Beye, M., Sorgenfrei, F., Turner, J. J., Reis, D. A., Gerken, N., Lee, S., Lee, W. S., Hays, G., Acremann, Y., Abbey, B., Coffee, R., Messerschmidt, M., Hau-Riege, S. P., Lapertot, G., Lüning, J., Heimann, P., Soufli, R., Fernández-Perea, M., Rowen, M., Holmes, M., Molodtsov, S. L., Föhlisch, A. & Wurth, W. (2012). *Opt. Express*, **20**, 11396–11406.

Maltezopoulos, T., Cunovic, S., Wieland, M., Beye, M., Azima, A., Redlin, H., Krikunova, M., Kalms, R., Frühling, U., Budzyn, F., Wurth, W., Föhlisch, A. & Drescher, M. (2008). *New J. Phys.* **10**, 033026.

Nakajima, K., Joti, Y., Kayatama, K., Owada, S., Togashi, T., Abe, T., Kameshima, T., Okada, K., Sugimoto, T., Yamaga, M., Hatsui, T. & Yabashi, M. (2018). *J. Synchrotron Rad.* **25**. Accepted.

Owada, S., Togawa, K., Inagaki, T., Hara, T., Tanaka, T., Joti, Y., Koyama, T., Nakajima, K., Ohashi, H., Senba, Y., Togashi, T., Tono, K., Yamaga, M., Yumoto, H., Yabashi, M., Tanaka, H. & Ishikawa, T. (2018). *J. Synchrotron Rad.* **25**, 282–288.

Sato, T., Togashi, T., Ogawa, K., Katayama, T., Inubushi, Y., Tono, K. & Yabashi, M. (2015). *Appl. Phys. Expr.* **8**, 012702.